Dynamical interactions between two uniformly magnetized spheres

Boyd F. Edwards
Department of Physics
Utah State University
Logan, UT 84322

John M. Edwards
Department of Informatics and Computer Science
Idaho State University
Pocatello, ID 83209

(Dated: September 5, 2016)

Studies of the two-dimensional motion of a magnet sphere in the presence of a second, fixed sphere provide a convenient venue for exploring magnet-magnet interactions, inertia, friction, and rich nonlinear dynamical behavior. These studies exploit the equivalence of these magnetic interactions to the interactions between two equivalent point dipoles. We show that magnet-magnet friction plays a role when magnet spheres are in contact, table friction plays a role at large sphere separations, and eddy currents are always negligible. Web-based simulation and visualization software, called *MagPhyx*, is provided for education, exploration, and discovery.

I. INTRODUCTION

Small neodymium magnet spheres are used both in and out of the classroom to teach principles of mathematics, physics, chemistry, biology, and engineering [1, 2]. They offer engaging hands-on exposure to principles of magnetism and are particularly useful in studying lattice structures, where they offer greater versatility than standard ball-and-stick models because they can connect at a continuous range of angles. They have spawned a learning community dedicated to sharing photos and tutorials of magnetic sculptures, some made from thousands of magnets, including models of molecules, fractals, and Platonic solids [3]. YouTube magnet sphere videos have attracted over a hundred million views [4].

A recent paper presents simple pedagogical arguments that confirm that the force between two uniformly magnetized spheres is identical to the force between two equivalent point magnetic dipoles, and confirms the same equivalence for the torque [5].

In this paper, we exploit this equivalence to investigate the dynamical interactions between two uniformly magnetized spheres, both with and without friction. We present tools intended to help students develop a better understanding of the forces and torques between magnets, and of their intimate relationship with the energy of interaction. These tools include instructive figures and discussions, and a web-based simulation tool called *MagPhyx* that enables students to animate the 2D motion of a uniformly magnetized sphere in response to the forces and torques produced by another sphere that is fixed in space. Explicit visualization of the magnetic field, force, torque, velocity, and angular velocity of the free sphere enables students to deepen their understanding of the role of inertia in magnet-magnet interactions. We have fully validated this software to ensure that it matches the dynamical equations of motion, and offer this simulation freely to the physics community [6].

This software fills a need. Online forums discuss the need for physically correct simulations of magnet-magnet interactions and lament the lack of closed form solutions for the forces between magnets [7–9]. The two-sphere problem is a good place to start with such simulations, thanks to the mathematical simplicity arising from the point-sphere equivalence. Commercial magnetic field mapping programs do not include simulations of magnet-magnet interactions [10], nor does the PhET suite of interactive physics simulation software [11]. As seen below, *MagPhyx* is a valuable exploration tool as well, revealing rich nonlinear behavior that will be the subject of future investigations.

The study of the motion of charged particles in a magnetic field in introductory physics courses can leave students with the false impression that magnetic fields do no work. It is true that magnetic fields do no work on charged particles. But magnetic fields do work on magnetic dipoles, translating and rotating them in fascinating ways, as discussed below.

One surprising property of small neodymium magnet spheres is how they generally find a way to attract each other. Placed in a repulsive configuration that might seem to lead to separation of two or more magnets, the magnets tend to twist and move until they attract and are drawn together. In years of informal experience with Zen Magnets (one brand of 5-mm diameter neodymium magnet spheres [12, 13]), we do not recall observing an initial configuration whose magnetic repulsion led eventually to separation of two or more magnets. We investigate non-conservative forces as possible mechanisms for this eventual attraction.

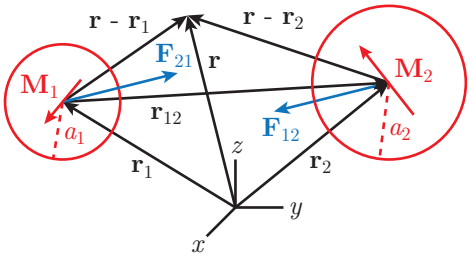

FIG. 1. Diagram showing two uniformly magnetized spheres with positions $\mathbf{r}_1$ and $\mathbf{r}_2$, radii a_1 and a_2, magnetizations $\mathbf{M}_1$ and $\mathbf{M}_2$, and paired non-central magnetic forces $\mathbf{F}_{12}$ and $\mathbf{F}_{21}$. Shown also are an arbitrary position vector $\mathbf{r}$ and the relative position vectors $\mathbf{r}-\mathbf{r}_1$, $\mathbf{r}-\mathbf{r}_2$, and $\mathbf{r}_{12}=\mathbf{r}_2-\mathbf{r}_1$. The same diagram applies for the forces between two point dipoles if spheres $\mathbf{M}_1$ and $\mathbf{M}_2$ are replaced by equivalent point dipoles $\mathbf{m}_1$ and $\mathbf{m}_2$ at the same locations.

In the sections that follow, we review the magnetic interactions between two uniformly magnetized spheres (Sec. II), illustrate these interactions in a 2D geometry with one sphere fixed at the origin and the other free to move in a plane (Sec. III), consider non-conservative forces (Sec. IV), write dimensionless variables to simplify numerical implementation (Sec. V), consider special cases to evaluate the role of non-conservative forces (Sec. VI), introduce and validate *MagPhyx* software by comparing its predictions for these special cases (Sec. VII), and summarize (Sec. VIII).

II. MAGNETIC INTERACTIONS

We here review the magnetic interactions between two uniformly magnetized spheres with arbitrary sizes, positions, magnetizations, and orientations [5]. Sphere i has position vector $\mathbf{r}_i$, radius a_i, magnetization $\mathbf{M}_i$, and total magnetic dipole moment

$$\mathbf{m}_i = \frac{4}{3}\pi a_i^3 \mathbf{M}_i, \tag{1}$$

where $i=1$, 2 (Fig. 1).

Outside of sphere i (for $|\mathbf{r}-\mathbf{r}_i|>a_i$), its magnetic field is given by [14, 15]

$$\mathbf{B}_i(\mathbf{r}) = \mathbf{B}(\mathbf{m}_i;\mathbf{r}-\mathbf{r}_i), \tag{2}$$

where $\mathbf{r}-\mathbf{r}_i$ is the position vector relative to the sphere center, and where

$$\mathbf{B}(\mathbf{m};\mathbf{r}) = \frac{\mu_0}{4\pi}\left(\frac{3\mathbf{m}\cdot\mathbf{r}}{r^5}\mathbf{r}-\frac{\mathbf{m}}{r^3}\right) \tag{3}$$

is the field of a dipole $\mathbf{m}$ located at the origin, in SI units [16, 17].

The interaction energy between sphere 2 and the magnetic field produced by sphere 1 is given by

$$U_{12} = -\mathbf{m}_2\cdot\mathbf{B}_1(\mathbf{r}_2) \tag{4}$$

$$= \frac{\mu_0}{4\pi}\left[\frac{\mathbf{m}_1\cdot\mathbf{m}_2}{{r_{12}}^3} - 3\frac{(\mathbf{m}_1\cdot\mathbf{r}_{12})(\mathbf{m}_2\cdot\mathbf{r}_{12})}{{r_{12}}^5}\right], \tag{5}$$

where $\mathbf{r}_{12}=\mathbf{r}_2-\mathbf{r}_1$ is the vector from sphere 1 to sphere 2, and $\mathbf{B}_1(\mathbf{r}_2)$ is the field produced by sphere 1 evaluated at the center of sphere 2.

The force of sphere 1 on sphere 2 follows as

$$\mathbf{F}_{12} = -\boldsymbol{\nabla}_2 U_{12} \tag{6}$$

$$= \frac{3\mu_0}{4\pi {r_{12}}^5}\Big[(\mathbf{m}_1\cdot\mathbf{r}_{12})\,\mathbf{m}_2 + (\mathbf{m}_2\cdot\mathbf{r}_{12})\,\mathbf{m}_1 + (\mathbf{m}_1\cdot\mathbf{m}_2)\,\mathbf{r}_{12} - 5\frac{(\mathbf{m}_1\cdot\mathbf{r}_{12})\,(\mathbf{m}_2\cdot\mathbf{r}_{12})}{{r_{12}}^2}\mathbf{r}_{12}\Big]. \tag{7}$$

Here, $\boldsymbol{\nabla}_2$ is the gradient with respect to $\mathbf{r}_2$. $\mathbf{F}_{12}$ is conservative but not central, namely, it is not generally parallel to the vector $\mathbf{r}_{12}$ between the dipoles (Fig. 1).

The torque of sphere 1 on sphere 2 is given by

$$\boldsymbol{\tau}_{12} = \mathbf{m}_2\times\mathbf{B}_1(\mathbf{r}_2) \tag{8}$$

$$= \frac{\mu_0}{4\pi}\left(\frac{3\mathbf{m}_1\cdot\mathbf{r}_{12}}{{r_{12}}^5}\mathbf{m}_2\times\mathbf{r}_{12} + \frac{\mathbf{m}_1\times\mathbf{m}_2}{{r_{12}}^3}\right). \tag{9}$$

Energy considerations assist in the understanding of the forces and torques on uniformly magnetized spheres. The force $\mathbf{F}_{12}=-\boldsymbol{\nabla}_2 U_{12}$ acts in the direction of maximum *decrease* of the energy $U_{12}=-\mathbf{m}_2\cdot\mathbf{B}_1(\mathbf{r}_2)$, that is, $\mathbf{F}_{12}$ acts in the direction of maximum *increase* in $\mathbf{m}_2\cdot\mathbf{B}_1$. In other words, $\mathbf{F}_{12}$ is in the direction of the virtual displacement of $\mathbf{m}_2$ that gives the largest increase in $\mathbf{m}_2\cdot\mathbf{B}_1 = m_2 B_1\cos\beta$, where β is the angle between $\mathbf{m}_2$ and $\mathbf{B}_1$. Equations (5) and (7) enable us to write the radial component of $\mathbf{F}_{12}$ in the simple form

$$F_{12}^r = \hat{\mathbf{r}}_{12}\cdot\mathbf{F}_{12} = \frac{3U_{12}}{r_{12}}, \tag{10}$$

where $\hat{\mathbf{r}}_{12}=\mathbf{r}_{12}/r_{12}$ is the unit vector in the direction of $\mathbf{r}_{12}$. Because m_2 and B_1 are both non-negative magnitudes, acute angles $\beta<\pi/2$ imply negative energies $U_{12}=-m_2B_1\cos\beta$ and attractive forces ($F_{12}^r<0$) that increase $\mathbf{m}_2\cdot\mathbf{B}_1>0$ by drawing $\mathbf{m}_2$ closer to $\mathbf{m}_1$ where the fields are *stronger*. Obtuse angles $\beta>\pi/2$ imply positive energies $U_{12}=-m_2B_1\cos\beta$ and repulsive forces ($F_{12}^r>0$) that increase $\mathbf{m}_2\cdot\mathbf{B}_1<0$ by pushing $\mathbf{m}_2$ away from $\mathbf{m}_1$ into regions with *weaker* fields.

III. 2D GEOMETRY

It is instructive to consider the interactions between two identical magnet spheres whose positions and magnetic orientations are confined to the x-y plane. We consider the forces and torques on a free sphere (sphere 2, of radius a, mass $\tilde{m}$, and moment of inertia $I=2\tilde{m}a^2/5$

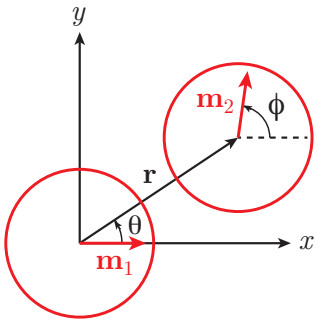

FIG. 2. Polar coordinate system used for 2D investigations of two spheres of the same radius. A sphere with magnetic moment $\mathbf{m}_1$ is held fixed at the origin with its magnetic moment in the $+x$ direction. A second sphere with magnetic moment $\mathbf{m}_2$ oriented at angle ϕ is located at position $\mathbf{r}$, with polar coordinates (r, θ).

[18]) in the x-y plane arising from the fields produced by a sphere (sphere 1, also of radius a) that is fixed at the origin ($\mathbf{r}_1 = 0$), with fixed dipole moment $\mathbf{m}_1 = m\hat{\mathbf{x}}$. We use polar coordinates (r, θ) to describe the position $\mathbf{r} = \mathbf{r}_2 = \mathbf{r}_{12} = r\cos\theta\,\hat{\mathbf{x}} + r\sin\theta\,\hat{\mathbf{y}}$ of the center of the free sphere, and angle ϕ to describe the angle of orientation of its dipole moment, $\mathbf{m}_2 = m\cos\phi\,\hat{\mathbf{x}} + m\sin\phi\,\hat{\mathbf{y}}$ (Fig. 2). The velocity and acceleration of the free sphere are given by $\mathbf{v} = \dot{\mathbf{r}}$ and $\mathbf{a} = \dot{\mathbf{v}}$, while its angular velocity and angular acceleration are given by $\boldsymbol{\omega} = \dot{\phi}\hat{\mathbf{z}}$ and $\boldsymbol{\alpha} = \dot{\boldsymbol{\omega}}$, where the overdot denotes a time derivative.

The 2D dynamics of the free sphere is characterized by the coordinates r, θ, and ϕ, and the corresponding momenta

$$p_r = \tilde{m}\dot{r} \tag{11}$$

$$p_\theta = \tilde{m}r^2\dot{\theta} \tag{12}$$

$$p_\phi = I\dot{\phi}, \tag{13}$$

which represent radial momentum, angular momentum, and spin angular momentum, respectively. The kinetic energy is

$$T = \frac{\tilde{m}}{2}\dot{r}^2 + \frac{\tilde{m}}{2}r^2\dot{\theta}^2 + \frac{I}{2}\dot{\phi}^2 \tag{14}$$

$$= \frac{p_r^2}{2\tilde{m}} + \frac{p_\theta^2}{2\tilde{m}r^2} + \frac{p_\phi^2}{2I}. \tag{15}$$

Figure 3 illustrates the principles discussed in Sec. II. It shows the dipole magnetic field $\mathbf{B}_1$ produced by the fixed sphere together with the magnetic forces and torques on the free sphere, for various positions and orientations of this sphere [19]. The forces fall into five categories, which are characterized by the angle β between $\mathbf{m}_2$ and $\mathbf{B}_1$.

1. *Attractive, Central* ($\beta = 0$): The force between two spheres is attractive and central when $\mathbf{m}_1$ and $\mathbf{m}_2$ are parallel and collinear [Fig. 3(a) A, E], leading to a stable equilibrium state with the north pole of one magnet contacting the south pole of the other. The force is also attractive and central when $\mathbf{m}_1$ and $\mathbf{m}_2$ are antiparallel to each other and perpendicular to the line through their centers [Fig. 3(e) C, G]. In both cases, $\mathbf{m}_2$ is parallel to $\mathbf{B}_1$ ($\beta = 0$), giving $\boldsymbol{\tau}_{12} = 0$ and $\mathbf{m}_2 \cdot \mathbf{B}_1 = mB_1$. To increase this positive product, $\mathbf{m}_1$ attracts $\mathbf{m}_2$ into its vicinity, where its field is stronger.

2. *Attractive, Oblique* ($0 < \beta < \pi/2$): For acute values of β, the force is attractive and non-central [Fig. 3(a) B, D, F, and H; Fig. 3(b) A, B, E, and F; Fig. 3(c) B, F; Fig. 3(d) B, C, F, and G]. The force acts to increase $\mathbf{m}_2 \cdot \mathbf{B}_1 = mB_1\cos\beta$ by moving $\mathbf{m}_2$ into regions where the field is stronger (larger B_1) and better aligned with $\mathbf{m}_2$ (smaller β, larger $\cos\beta$). The torque also acts to increase $\mathbf{m}_2 \cdot \mathbf{B}_1$ by rotating $\mathbf{m}_2$ into alignment with $\mathbf{B}_1$.

3. *Perpendicular* ($\beta = \pi/2$): When $\mathbf{m}_2$ is perpendicular to $\mathbf{B}_1$, the force of $\mathbf{m}_1$ on $\mathbf{m}_2$ is perpendicular to the line joining these spheres – it is neither attractive nor repulsive [Fig. 3(c) A, C, E, and G]. This force acts to increase $\mathbf{m}_2 \cdot \mathbf{B}_1$ by moving $\mathbf{m}_2$ toward a region where it is better aligned with the field. The torque again acts to rotate $\mathbf{m}_2$ into alignment with $\mathbf{B}_1$.

4. *Repulsive, Oblique* ($\pi/2 < \beta < \pi$): For obtuse values of β, the force is repulsive and non-central [Fig. 3(b) C, D, G, and H; Fig. 3(c) D, H; Fig. 3(d) A, D, E, and H; Fig. 3(e) B, D, F, and H]. The force acts to increase the negative product $\mathbf{m}_2 \cdot \mathbf{B}_1 = -mB_1|\cos\beta|$ (that is, to bring it closer to zero) by moving $\mathbf{m}_2$ into regions where the field is weaker (smaller B_1) and better aligned with $\mathbf{m}_2$ (β approaching $\pi/2$ from above, smaller $|\cos\beta|$). The torque acts to increase $\mathbf{m}_2 \cdot \mathbf{B}_1$ by rotating $\mathbf{m}_2$ into alignment with the local field.

5. *Repulsive, Central* ($\beta = \pi$): The force is repulsive and central when $\mathbf{m}_1$ and $\mathbf{m}_2$ are parallel to each other and perpendicular to the line through their centers [Fig. 3(a) C, G], and when $\mathbf{m}_1$ and $\mathbf{m}_2$ are antiparallel and collinear [Fig. 3(e) A, E]. In both cases, $\mathbf{m}_2$ is antiparallel to $\mathbf{B}_1$ ($\beta = \pi$), giving $\boldsymbol{\tau}_{12} = 0$ and $\mathbf{m}_2 \cdot \mathbf{B}_1 = -mB_1$. To increase this negative product, $\mathbf{m}_1$ repels $\mathbf{m}_2$ into regions where the field is weaker.

These five categories are useful in characterizing the magnetic interactions between spheres; we found ourselves consulting Fig. 3 often as we explored these interactions.

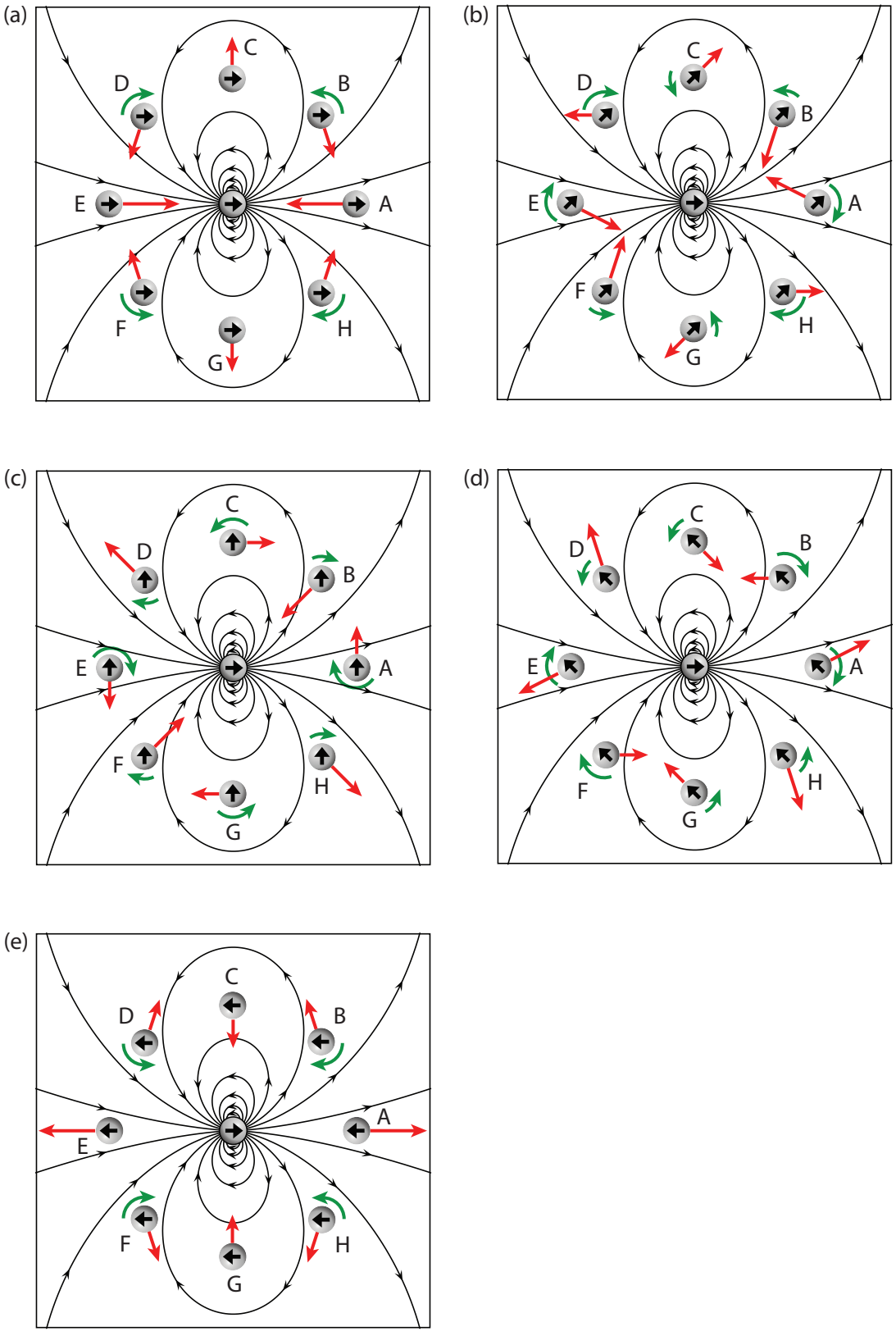

FIG. 3. Magnetic field lines produced by a uniformly magnetized sphere of total magnetic moment $\mathbf{m}_1$ [Eq. (1)], at the center of each panel, and the resulting magnetic forces and torques on a uniformly magnetized sphere of total magnetic moment $\mathbf{m}_2$, at various positions and orientations, as given by Eqs. (3), (7), and (9). Shown are drawings for $\mathbf{m}_2$ and $\mathbf{m}_1$ differing by angles 0 (a), $\pi/4$ (b), $\pi/2$, (c) $3\pi/4$ (d), and π (e). For each panel, there are eight positions of sphere 2, labeled A-H, spaced evenly around a circle centered on sphere 1. Force vectors are shown with their lengths proportional to the force magnitude. Torques are indicated by clockwise and counterclockwise circular arcs, with the arc length increasing with torque magnitude, and with no arc if the torque is zero. The directions of the magnetic moments are indicated by bold arrows centered on the sphere images.

IV. NONCONSERVATIVE FORCES

Magnets sliding across a table top or sliding against each other experience kinetic friction forces, and electrically conducting magnets moving through a magnetic field experience eddy forces. Because these forces can dissipate energy, they may help to explain why magnets tend to attract rather than repel.

A. Kinetic Friction

Kinetic friction dissipates energy for objects that slide along a surface such as a horizontal table top. The downward gravitational force $\tilde{m}g$ on a sliding magnet sphere equals the upward normal force on it, and a table friction force

$$\mathbf{f}_t = -\mu_t \tilde{m} g \hat{\mathbf{v}} \tag{16}$$

on the sphere is directed opposite to its direction of motion $\hat{\mathbf{v}} = \mathbf{v}/v$ along the table. Here, μ_t is the coefficient of kinetic friction between a magnet and the table, g is the local acceleration of gravity, and $\tilde{m}$ is the sphere mass.

Similarly, a table exerts a frictional torque

$$\boldsymbol{\tau}_t = -\mu_t^* \tilde{m} g D \hat{\boldsymbol{\omega}} \tag{17}$$

on a magnet that is spinning on the table, where μ_t^* is the associated coefficient of friction and D is the sphere diameter. This torque is directed opposite to the direction $\hat{\boldsymbol{\omega}} = \boldsymbol{\omega}/\omega$ of the spin of the sphere, assumed to be perpendicular to the table.

Kinetic friction can also occur between two magnet spheres that are sliding against each other. If sphere 1 is held fixed at the origin, such sliding can occur because sphere 2 is rotating but not translating, because sphere 2 is translating along the surface of sphere 1 without rotating, or because sphere 2 is both translating and rotating. The associated magnet-magnet friction force

$$\mathbf{f}_m = -\mu_m \mathrm{F_N} \hat{\mathbf{v}}_t \tag{18}$$

of sphere 1 on sphere 2 is directed opposite to the tangential velocity vector $\mathbf{v}_t = \mathbf{v} - a\boldsymbol{\omega} \times \hat{\mathbf{r}}$ of sphere 2 at its point of contact with sphere 1, where $\mathbf{f}_m$ is applied. Here, $\hat{\mathbf{r}} = \mathbf{r}/r$ is a unit position vector, $\hat{\mathbf{v}}_t = \mathbf{v}_t/v_t$ is a unit tangential velocity vector, $\mathrm{F_N}$ is the magnitude of the normal force of sphere 1 on sphere 2, μ_m is the coefficient of kinetic friction between the two spheres, and $-a\hat{\mathbf{r}}$ is the location of the sphere-sphere contact point relative to the center of sphere 2. Since $\mathbf{f}_m$ is applied along the tangent to the surface of sphere 2, it also exerts a torque

$$\boldsymbol{\tau}_m = -a\hat{\mathbf{r}} \times \mathbf{f}_m \tag{19}$$

on that sphere.

These kinetic friction forces are proportional to the applicable normal force, which is the force of gravity in the case of table friction, and includes the radial component of the magnetic force in the case of magnet-magnet friction. Given that magnetic forces between two magnets that are in contact with each other typically exceed gravitational forces on these magnets, magnet-magnet friction dominates when magnets are in contact.

B. Eddy Currents

We also investigate eddy currents as a possible damping mechanism. An object with conductivity σ that moves with velocity $\mathbf{v}$ through a static magnetic field experiences eddy currents with current density $\mathbf{J} = \sigma\mathbf{E}$, where $\mathbf{E} = \mathbf{v} \times \mathbf{B}$ is the motional electric field [20]. These currents act to oppose the change in magnetic flux, and produce an eddy force $\mathbf{F}^{\mathrm{eddy}} = \int \mathbf{J} \times \mathbf{B}\, dV$ on the conductor, where the integral is over the volume of the conductor. Thus

$$\mathbf{F}^{\mathrm{eddy}} = \int \sigma\, (\mathbf{v} \times \mathbf{B}) \times \mathbf{B}\; dV \tag{20}$$

$$= -\mathbf{v} \int \sigma B^2 dV + \int \sigma\, (\mathbf{v} \cdot \mathbf{B})\, \mathbf{B}\, dV. \tag{21}$$

The component of this force in the direction of the velocity is given by

$$\hat{\mathbf{v}} \cdot \mathbf{F}^{\mathrm{eddy}} = -v \int \sigma B^2 dV + v \int \sigma\, (\hat{\mathbf{v}} \cdot \mathbf{B})^2\, dV, \tag{22}$$

where $\hat{\mathbf{v}} = \mathbf{v}/v$ is the unit vector in the direction of $\mathbf{v}$. Unless $\mathbf{v}$ is parallel to $\mathbf{B}$ or antiparallel to $\mathbf{B}$ throughout the volume of the conductor, the first term dominates and $\hat{\mathbf{v}} \cdot \mathbf{F}^{\mathrm{eddy}} < 0$.

To make an order-of-magnitude assessment of the eddy currents produced in sphere 2 as it moves through the static field of sphere 1, held fixed, we ignore the second term of Eq. (21) and replace B^2 in the integrand of the first term with its value $B_1^2(\mathbf{r})$ at the center of sphere 2, yielding the simple, approximate result

$$\mathbf{F}^{\mathrm{eddy}} = -\frac{4}{3}\pi a^3 \bar{\sigma} B_1^2(\mathbf{r})\, \mathbf{v}. \tag{23}$$

In this approximation, the eddy force $\mathbf{F}^{\mathrm{eddy}}$ of sphere 1 on sphere 2 is antiparallel to the velocity $\mathbf{v}$ of sphere 2, like the Stokes drag on a sphere moving slowly through a viscous fluid [21], and is proportional to the square of the local magnetic field.

Commercial neodymium magnets typically have spherical nickel-copper coatings that have significantly higher conductivities than their neodymium alloy interiors. To account for these coatings on the eddy forces, we write $\sigma = \sigma(\rho)$, where ρ is the radial position from the sphere center, and use the volume element $dV = 4\pi\rho^2 d\rho$ to calculate the average conductivity

$$\bar{\sigma} = \frac{\int \sigma(\rho) dV}{\int dV} = \frac{3}{a^3} \int_0^a \sigma(\rho) \rho^2 d\rho, \tag{24}$$

which appears in Eq. (23).

Zen Magnets have neodymium-iron-boron alloy ($Nd_2Fe_{14}B$) interiors of radius 2.450 mm and conductivity $\sigma_a = 6.67 \times 10^5\ \Omega^{-1}\ \mathrm{m}^{-1}$ surrounded by a 0.015-mm layer of nickel with conductivity $\sigma_n = 1.43 \times 10^7\ \Omega^{-1}\ \mathrm{m}^{-1}$, a 0.025-mm layer of copper with conductivity $\sigma_c = 5.96 \times 10^7\ \Omega^{-1}\ \mathrm{m}^{-1}$, and a final 0.010-mm layer of nickel, for a total radius of 2.500 mm [22–25]. Accordingly, Eq. (24) gives

$$\bar{\sigma} = 2.80 \times 10^6\ \Omega^{-1}\ \mathrm{m}^{-1}. \tag{25}$$

Eddy currents also produce torques on spinning conductors in the presence of a magnetic field [26–28]. A conductor that rotates with angular velocity $\boldsymbol{\omega}$ in a magnetic field generates eddy currents with current density $\mathbf{J} = \sigma\mathbf{E}$, where the motional electric field $\mathbf{E} = \mathbf{v}\times\mathbf{B}$ relies on the rotational velocity $\mathbf{v} = \boldsymbol{\omega}\times\boldsymbol{\rho}$ of a point in sphere 2, located relative to the sphere center by the position vector $\boldsymbol{\rho}$ [29]. The force on a volume element is $\mathbf{J}\times\mathbf{B}\,dV$, and the associated torque is $d\boldsymbol{\tau} = \boldsymbol{\rho}\times(\mathbf{J}\times\mathbf{B})\,dV$, so the total torque on the sphere is

$$\boldsymbol{\tau}^{\mathrm{eddy}} = \int \boldsymbol{\rho}\times(\mathbf{J}\times\mathbf{B})\,dV. \tag{26}$$

This can be rewritten as

$$\boldsymbol{\tau}^{\mathrm{eddy}} = -\boldsymbol{\omega}\int\sigma B^2\rho^2\,dV + \int\sigma\Big[(\boldsymbol{\omega}\times\boldsymbol{\rho})\cdot\mathbf{B}\Big]\boldsymbol{\rho}\times\mathbf{B}\,dV. \tag{27}$$

The component of this torque in the direction of the angular velocity is

$$\hat{\boldsymbol{\omega}}\cdot\boldsymbol{\tau}^{\mathrm{eddy}} = -\omega\int\sigma\rho^2B^2dV + \omega\int\sigma\Big[(\hat{\boldsymbol{\omega}}\times\boldsymbol{\rho})\cdot\mathbf{B}\Big]^2dV, \tag{28}$$

where $\hat{\boldsymbol{\omega}} = \boldsymbol{\omega}/\omega$ is the unit vector in the direction of $\boldsymbol{\omega}$.

As before, the first term dominates, we ignore the second term of Eq. (27), and we replace B^2 in the integrand of the first term with its value $B_1^2(\mathbf{r})$ at the center of sphere 2, giving the approximate result

$$\boldsymbol{\tau}^{\mathrm{eddy}} = -\frac{4}{5}\pi a^5\sigma^* B_1^2(\mathbf{r})\,\boldsymbol{\omega}, \tag{29}$$

where

$$\sigma^* = \frac{\int\sigma(\rho)\rho^2dV}{\int\rho^2dV} = \frac{5}{a^5}\int_0^a\sigma(\rho)\rho^4dr \tag{30}$$

is the associated weighted average conductivity. In this approximation, the eddy torque is antiparallel to the angular velocity vector and is proportional to the square of the local magnetic field. Using the Zen Magnets data above, we obtain

$$\sigma^* = 4.16 \times 10^6\ \Omega^{-1}\ \mathrm{m}^{-1}. \tag{31}$$

In our simulations, we employ Eqs. (23) and (29) to describe the eddy force and torque on the free sphere, with Eqs. (25) and (31) providing estimates of the associated weighted conductivities.

C. Newtonian Formulation

To study the role of non-conservative forces on the 2D dynamics of sphere 2, it is convenient to use Newtonian dynamics. Applied to sphere 2 (with sphere 1 held fixed at the origin), Newton's second law states

$$\mathbf{F}_{12} + \mathbf{f}_t + \mathbf{f}_m + \mathbf{F}^{\mathrm{eddy}} + \mathbf{F}_{\mathrm{N}} = \tilde{m}\mathbf{a}, \tag{32}$$

with terms on the left side given by Eqs. (7), (16), (18), and (23) and a final term giving the normal force of the fixed sphere on the free sphere. The forces $\mathbf{f}_m$ and $\mathbf{F}_{\mathrm{N}}$ apply only when the magnets are in contact. Newton's second law for rotations states

$$\boldsymbol{\tau}_{12} + \boldsymbol{\tau}_t + \boldsymbol{\tau}_m + \boldsymbol{\tau}^{\mathrm{eddy}} = I\boldsymbol{\alpha}, \tag{33}$$

with terms given by Eqs. (9), (17), (19), and (29).

V. DIMENSIONLESS VARIABLES

To simplify calculations, we scale length by the magnet diameter $D = 2a$, force by $F_0 = 3\mu_0m^2/(2\pi D^4)$, energy and torque by F_0D, time by $T_0 = \sqrt{\tilde{m}D/F_0}$, magnetic field by F_0D/m, magnetic moment by m, velocity by D/T_0, acceleration by D/T_0^2, angular velocity by T_0^{-1}, angular acceleration by T_0^{-2}, radial (linear) momentum by $\tilde{m}D/T_0$, and orbital and spin angular momentum by $\tilde{m}D^2/T_0$. Here, F_0 is the force between two magnets in the minimum-energy state with the north pole of one touching the south pole of the other, and T_0 is the time scale for the magnetic force to bring two magnets together starting from rest at separations of the order of $2D$. In dimensionless units, the magnet diameter and the center-to-center distance between touching magnets are both 1, and the magnetic moment vectors are unit vectors.

In dimensionless variables in the 2D geometry described in Sec. III, Eq. (3) has the dimensionless form

$$\mathbf{B}_1 = \frac{1}{12r^3}\Big[(1+3\cos2\theta)\,\hat{\mathbf{x}} + 3\sin2\theta\,\hat{\mathbf{y}}\Big], \tag{34}$$

which has magnitude

$$B_1(r,\theta) = \frac{1}{12r^3}\,(10+6\cos2\theta)^{1/2} \tag{35}$$

and direction ϕ_m (measured counterclockwise from the $+x$ direction) given by

$$\tan\phi_m = \frac{3\sin2\theta}{1+3\cos2\theta}. \tag{36}$$

Equations (5), (15), (11)-(13), and (32) become

$$E = T + U \tag{37}$$

$$U = -\frac{1}{12r^3}\Big[\cos\phi + 3\cos(\phi - 2\theta)\Big] \tag{38}$$

$$T = \frac{p_r^2}{2} + \frac{p_\theta^2}{2r^2} + 5p_\phi^2 \tag{39}$$

$$p_r = \dot{r} \tag{40}$$

$$p_\theta = r^2\dot{\theta} \tag{41}$$

$$p_\phi = \dot{\phi}/10 \tag{42}$$

$$\frac{d\mathbf{v}}{dt} = \mathbf{F}_{12} + \mathbf{f}_t + \mathbf{f}_m + \mathbf{F}^{\rm eddy} + \mathbf{F}_{\rm N}, \tag{43}$$

where E is the total energy, and where

$$\mathbf{F}_{12} = -\frac{1}{4r^4}\Big[\cos\phi + 3\cos(\phi - 2\theta)\Big]\,\hat{\mathbf{r}} + \frac{1}{2r^4}\sin(\phi - 2\theta)\,\hat{\boldsymbol{\theta}} \tag{44}$$

$$\mathbf{f}_t = -\gamma\hat{\mathbf{v}} \tag{45}$$

$$\mathbf{f}_m = -\mu_m \mathrm{F_N}\hat{\mathbf{v}}_t \tag{46}$$

$$\mathbf{F}^{\rm eddy} = -\eta B_1^2(\mathbf{r})\,\mathbf{v}. \tag{47}$$

Here, $\mathbf{f}_m$ and $\mathbf{F}_{\rm N}$ apply only when sphere 2 is in contact with sphere 1, that is, when $r = 1$, and $\hat{\mathbf{v}}_t = \mathbf{v}_t/v_t$ follows from the dimensionless tangential velocity vector,

$$\mathbf{v}_t = \mathbf{v} - \boldsymbol{\omega}\times\hat{\mathbf{r}}/2. \tag{48}$$

The total energy E is conserved if the magnetic force $\mathbf{F}_{12} = -\boldsymbol{\nabla}_2 U_{12}$ only is included in Eq. (43); E is a decreasing function of time otherwise.

Equation (44) is resolved into components in the polar directions

$$\hat{\mathbf{r}} = \cos\theta\,\hat{\mathbf{x}} + \sin\theta\,\hat{\mathbf{y}} \tag{49}$$

$$\hat{\boldsymbol{\theta}} = -\sin\theta\,\hat{\mathbf{x}} + \cos\theta\,\hat{\mathbf{y}} \tag{50}$$

In polar coordinates,

$$\mathbf{v} = \frac{d\mathbf{r}}{dt} = \dot{r}\hat{\mathbf{r}} + r\dot{\theta}\hat{\boldsymbol{\theta}} \tag{51}$$

and

$$\mathbf{a} = \frac{d\mathbf{v}}{dt} = \left(\ddot{r} - r\dot{\theta}^2\right)\hat{\mathbf{r}} + \frac{1}{r}\frac{d}{dt}\left(r^2\dot{\theta}\right)\hat{\boldsymbol{\theta}} \tag{52}$$

The dimensionless coefficients

$$\gamma = \frac{2\pi\mu_t\tilde{m}gD^4}{3\mu_0 m^2} \tag{53}$$

$$\eta = \frac{1}{4}\mu_0\bar{\sigma}m\sqrt{\frac{3\mu_0}{2\pi\tilde{m}D}} \tag{54}$$

respectively characterize the strength of table friction and eddy forces. Zen Magnets near the earth's surface have $D = 5$ mm, $m = 0.05$ A·m^2, $\tilde{m} = 0.5$ g, $g = 9.8$ m/s^2, $\mu_0 = 4\pi\times10^{-7}$ N/A^2, and $\bar{\sigma} = 2.80\times10^6\ \Omega^{-1}$ m^{-1} [Eq. (25)] [2]. Kinetic friction coefficients generally lie between 0 and 1. In order to give a rough idea of the role of table friction for a variety of table surfaces, we simply take $\mu_t = 0.5$. Inserting these values gives $\gamma = 0.001$ and $\eta = 0.02$. For magnet-magnet friction, we take

$$\mu_m = 0.53, \tag{55}$$

pertinent to nickel on nickel [30].

Equation (33) has the dimensionless form

$$\frac{1}{10}\frac{d\boldsymbol{\omega}}{dt} = \boldsymbol{\tau}_{12} + \boldsymbol{\tau}_t + \boldsymbol{\tau}_m + \boldsymbol{\tau}^{\rm eddy}, \tag{56}$$

with

$$\boldsymbol{\tau}_{12} = -\frac{1}{12r^3}\Big[\sin\phi + 3\sin(\phi - 2\theta)\Big]\hat{\mathbf{z}} \tag{57}$$

$$\boldsymbol{\tau}_t = -\gamma^*\hat{\boldsymbol{\omega}} \tag{58}$$

$$\boldsymbol{\tau}_m = -\hat{\mathbf{r}}\times\mathbf{f}_m/2 \tag{59}$$

$$\boldsymbol{\tau}^{\rm eddy} = -\eta^* B_1^2(\mathbf{r})\,\boldsymbol{\omega}, \tag{60}$$

where $\boldsymbol{\tau}_m$ applies only when sphere 2 is in contact with sphere 1, that is, when $r = 1$.

The dimensionless coefficients

$$\gamma^* = \frac{2\pi\mu_t^*\tilde{m}gD^4}{3\mu_0 m^2} \tag{61}$$

$$\eta^* = \frac{3}{80}\mu_0\sigma^* m\sqrt{\frac{3\mu_0}{2\pi\tilde{m}D}} \tag{62}$$

respectively characterize the strength of table friction and eddy torques. Inserting $\mu_t^* = 0.5$ and $\sigma^* = 4.16\times10^6\ \Omega^{-1}$ m^{-1} from Eq. (31) gives $\gamma^* = 0.001$ and $\eta^* = 0.005$.

We can now combine the considerations in this section to cast Eqs. (43) and (56) as a system of first-order equations governing the dynamical variables r, θ, ϕ, p_r, p_θ, and p_ϕ,

$$\dot{r} = p_r \tag{63}$$

$$\dot{\theta} = \frac{p_\theta}{r^2} \tag{64}$$

$$\dot{\phi} = 10p_\phi \tag{65}$$

$$\dot{p}_r = \frac{p_\theta^2}{r^3} + \frac{3U}{r} - \tilde{f}p_r + \mathrm{F_N} \tag{66}$$

$$\dot{p}_\theta = \frac{1}{2r^3}\sin(\phi - 2\theta) - \tilde{f}p_\theta + \frac{5\mu_m \mathrm{F_N}}{v_t}rp_\phi \tag{67}$$

$$\dot{p}_\phi = -\frac{1}{12r^3}\Big[\sin\phi + 3\sin(\phi - 2\theta)\Big] - \tilde{\tau}p_\phi + \frac{\mu_m \mathrm{F_N}}{2v_t}p_\theta \tag{68}$$

where

$$\tilde{f} = \frac{\gamma}{v} + \eta B_1^2 + \frac{\mu_m \mathrm{F_N}}{v_t} \tag{69}$$

$$\tilde{\tau} = \frac{\gamma^*}{|p_\phi|} + 10\eta^* B_1^2 + \frac{5\mu_m \mathrm{F_N}}{2v_t} \tag{70}$$

are combined frictional forces and torques, and where

$$v = \left(p_r^2 + p_\theta^2/r^2\right)^{1/2} \tag{71}$$

$$v_t = \left[p_r^2 + (p_\theta - 5p_\phi)^2\right]^{1/2} \tag{72}$$

are the speed of sphere 2 and the tangential speed of its point of contact with sphere 1, if applicable. The terms involving $\mathrm{F_N}$ are included only if the spheres are in contact, for which $r = 1$, $p_r = 0$, and

$$\mathrm{F_N} = -3U - p_\theta^2 \tag{73}$$

is chosen to satisfy $\dot{p}_r = 0$ in Eq. (66). Consequently, $U < -p_\theta^2/3$ must hold lest $\mathrm{F_N} < 0$ and sphere 2 lose contact with sphere 1. Equations (35) and (38) may be used to evaluate B_1 and U.

Dimensionless variables are used in all equations in this and subsequent sections, and in all figures in the manuscript except for Fig. 1.

VI. SPECIAL CASES

Studying pure translations and pure rotations illustrates simple elements of the dynamics and allows us to investigate the role of frictional forces and torques.

A. Translation

We release sphere 2 from rest at $(r, \theta, \phi) = (x_0, 0, 0)$ (Fig. 3a A) and determine the elapsed time and speed at which it collides with sphere 1, which is held fixed at the origin. In this case, sphere 2 experiences no torque and moves in the $-x$ direction with time-dependent position $x(t)$ and velocity $v_x = dx/dt < 0$ obeying

$$\frac{dv_x}{dt} = -\frac{1}{x^4} + \gamma - \frac{\eta}{9x^6} v_x, \tag{74}$$

from Eq. (43). The terms on the right side give, from left to right, the attractive magnetic force of sphere 1 on sphere 2, the dissipative force of table friction, and the dissipative force of eddy friction.

Equation (74) can be integrated analytically in the absence of eddy friction ($\eta = 0$). Writing

$$\frac{dv_x}{dt} = \frac{dv_x}{dx}\frac{dx}{dt} = v_x \frac{dv_x}{dx} \tag{75}$$

enables us to cast Eq. (74) as

$$\int v_x dv_x = \int \left(\gamma - \frac{1}{x^4}\right) dx. \tag{76}$$

Integrating and applying the initial conditions $x(0) = x_0$ and $v_x(0) = 0$ gives

$$v_x(x) = -\left[\frac{2}{3}\left(\frac{1}{x^3} - \frac{1}{x_0^3}\right) + 2\gamma\,(x - x_0)\right]^{1/2}, \tag{77}$$

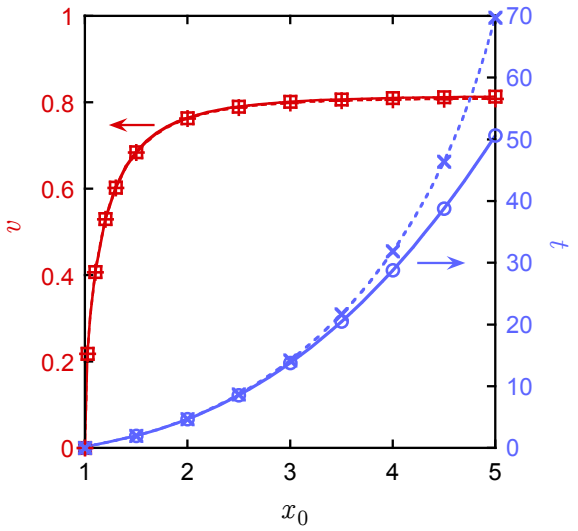

FIG. 4. Dimensionless collision speed v and elapsed time t for a uniformly magnetized sphere that is released from rest at initial position $x_0\hat{\mathbf{x}}$, and is attracted by a second uniformly magnetized sphere that is held fixed at the origin (Fig. 3a A). Both spheres have the same dipole moment, each pointed in the $+x$ direction. For v, the solid trace and the open squares are given respectively by Eq. (79) and *MagPhyx* software for $\gamma = 0$ (no table friction), and the dashed trace and the plus symbols are given by Eq. (79) and *MagPhyx* software for $\gamma = 0.001$ (table friction pertinent to Zen Magnets). For t, the solid trace and open circles are given by Eq. (78) and *MagPhyx* for $\gamma = 0$, and the dashed trace and the "×" symbols are given by Eq. (78) and *MagPhyx* for $\gamma = 0.001$.

which depends on time through $x = x(t)$. Inserting $v_x = dx/dt$ and integrating allows us to find the time at collision,

$$t = -\int_1^{x_0} v_x^{-1}(x) dx. \tag{78}$$

The integral is from $x = 1$, where the collision occurs, to $x_0 \geq 1$, the initial position of sphere 2. Equation (77) yields the corresponding speed $v = -v_x$ at the time of collision,

$$v = \left[\frac{2}{3}\left(1 - \frac{1}{x_0^3}\right) + 2\gamma\,(1 - x_0)\right]^{1/2}. \tag{79}$$

Figure 4 shows results for v and t as a function of x_0, for no table friction ($\gamma = 0$) and for table friction pertinent to Zen Magnets ($\gamma = 0.001$, Sec. V). For $x_0 = 1$, sphere 2 is initially in contact with sphere 1, and $v = t = 0$. As x_0 increases from 1, v increases rapidly at first and slowly thereafter, reflecting the rapid decay of the $1/r^4$ magnetic force with increasing sphere separation. The collision speed depends little on distance for large distances because the magnetic force is weak at large distances, and this force contributes little to final speed of sphere 2. On the other hand, t increases rapidly with increasing distance for large distances because sphere 2,

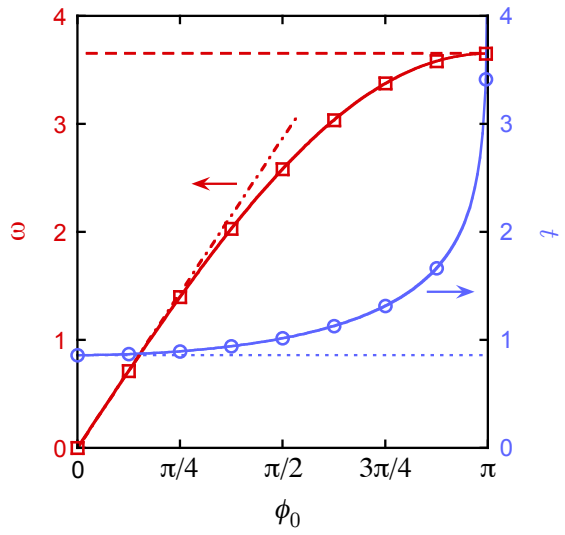

FIG. 5. Dimensionless angular speed ω and elapsed time t vs. initial angle ϕ_0 for a uniformly magnetized sphere that is allowed to spin freely without friction at a fixed location $x = 1$ and $y = 0$ in response to the magnetic torque from a second uniformly magnetized sphere that is held fixed at the origin, with dipole moment in the $+x$ direction. The spinning sphere is released from rest with its dipole moment oriented at an angle $\phi = \phi_0$ with respect to the $+x$ direction. The angular speed ω and elapsed time t pertain to the first zero crossing of ϕ. For ω, the solid trace and the squares are given respectively by Eq. (85) and *MagPhyx* software. For t, the solid trace and the circles are given by Eq. (84) and *MagPhyx*. The short-dashed and chain-dashed lines give the small-amplitude limits given by Eqs. (87) and (88), and the long-dashed line gives the large-amplitude limit given by Eq. (89).

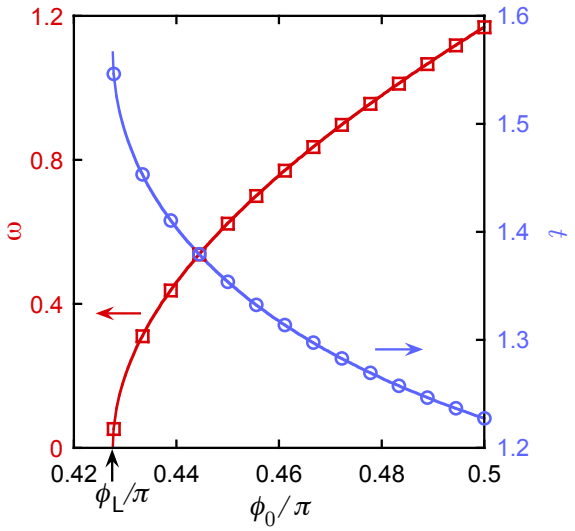

FIG. 6. Dimensionless angular speed ω and elapsed time t vs. initial angle ϕ_0 for a uniformly magnetized sphere that is allowed to spin at a fixed location $x = 1$ and $y = 0$ in response to the magnetic torque and the magnet-magnet friction torque with $\mu_m = 0.53$. For ω, the solid trace and the squares are given respectively by Eq. (85) and *MagPhyx*. For t, the solid trace and circles are given by Eq. (84) and *MagPhyx*. Also shown is the lower limit ϕ_L given by Eq. (90).

starting from rest, spends a lot of time traveling slowly before reaching the regions near sphere 1 where the force is strong. Values for t were obtained from Eq. (78) by numerical integration with $dx = 10^{-6}$.

Table friction is negligible for small x_0 because there the magnetic force overwhelms the table friction force. The role of friction on v remains negligible for $x_0 \approx 4$ because at these distances, table friction simply serves to oppose the magnetic force, which is already weak and plays little role in the collision speed. Table friction does play a role on the elapsed time for $x_0 \approx 4$, because it reduces the already small speed of sphere 2 at these distances, where most of the time is spent.

To investigate the role of eddy friction, we use the forward Euler method with $dt = 0.0001$ to integrate Eq. (74) and $v_x = dx/dt$ for $1 \le x_0 \le 5$. For $\eta = 0.02$ pertinent to Zen Magnets (Sec. V), eddy friction decreases v and increases t by less than 0.1%.

B. Rotation

We now consider rotation without translation. We confine sphere 2 to a fixed location on the $+x$ axis and allow it to spin freely about an axis through its center that is parallel to the z axis, in response to magnetic and frictional torques. We release it with zero initial angular velocity at an initial angle ϕ_0 and calculate both the time required for it to align itself with the magnetic field ($\phi = 0$) and its angular speed ω at that time. During this time, $\omega_z = d\phi/dt < 0$ and the sphere is subject to the torques of Eq. (56),

$$\frac{1}{10}\frac{d\omega_z}{dt} = -\frac{1}{3x^3}\sin\phi + \gamma^* + \frac{\mu_m}{2}\cos\phi - \frac{\eta^*}{9x^6}\omega_z. \quad (80)$$

The terms on the right side respectively represent the magnetic torque, the table friction torque, the magnet-magnet friction torque (applicable only when sphere 2 is in contact with sphere 1, and when the force between them is attractive), and the eddy torque.

Equation (80) can be solved analytically in the absence of the eddy torque ($\eta^* = 0$). We insert

$$\frac{d\omega_z}{dt} = \frac{d\omega_z}{d\phi}\frac{d\phi}{dt} = \omega_z\frac{d\omega_z}{d\phi} \quad (81)$$

into Eq. (80) and rewrite it to yield

$$\int \omega_z d\omega_z = 10\int\left(-\frac{1}{3x^3}\sin\phi + \gamma^* + \frac{\mu_m}{2}\cos\phi\right)d\phi. \quad (82)$$

Integrating and applying the initial conditions $\omega_z(0) = 0$

and $\phi(0) = \phi_0$ yields the angular velocity

$$\omega_z(\phi) = -2\sqrt{5}\Big[\frac{1}{3x^3}(\cos\phi - \cos\phi_0) + \gamma^*(\phi - \phi_0) + \frac{\mu_m}{2}(\sin\phi - \sin\phi_0)\Big]^{1/2}, \tag{83}$$

which depends on time through $\phi = \phi(t)$. Inserting $\omega_z = d\phi/dt$ and integrating gives

$$\int dt = -\int_0^{\phi_0} \omega_z^{-1}(\phi) d\phi. \tag{84}$$

Equation (83) yields the corresponding speed $\omega = -\omega_z$ at $\phi = 0$,

$$\omega = 2\sqrt{5}\left[\frac{1}{3x^3}(1 - \cos\phi_0) - \gamma^*\phi_0 - \frac{\mu_m}{2}\sin\phi_0\right]^{1/2}. \tag{85}$$

For $\phi_0 = \pi/2$, Eq. (85) gives

$$\omega = 2\sqrt{5}\left(\frac{1}{3x^3} - \frac{\pi}{2}\gamma^* - \frac{\mu_m}{2}\right)^{1/2}. \tag{86}$$

We first consider the frictionless case with $\gamma^* = \mu_m = 0$, which oscillates indefinitely about $\phi = 0$ with amplitude ϕ_0. For $x = 1$, small-amplitude oscillations ($\phi_0 \ll 1$) yield

$$t = \frac{\pi}{2}\sqrt{\frac{3}{10}} \tag{87}$$

and

$$\omega = \sqrt{\frac{10}{3}}\,\phi_0, \tag{88}$$

while large-amplitude oscillations ($\phi_0 \to \pi$) give $t \to \infty$ and

$$\omega = 2\sqrt{\frac{10}{3}}. \tag{89}$$

Figure 5 gives general results for $x = 1$ and $0 \le \phi_0 < \pi$, with values of t obtained from Eq. (84) by numerical integration with $d\phi = 10^{-6}$.

We next consider the role of friction. For $x = 1$ and values $\mu_m = 0.53$, $\gamma^* = 0.001$, and $\eta^* = 0.005$ pertinent to Zen Magnets (Sec. V), the magnitudes of terms in Eqs. (80) and (86) indicate that table friction, characterized by γ^*, and eddy friction, characterized by η^*, alter typical values of the force and the angular velocity by less than 1% when sphere 2 is in contact with sphere 1. But magnet-magnet friction, characterized by μ_m, is proportional to the magnet force between sphere 1 and sphere 2, and is non-negligible when these spheres are in contact. When magnet-magnet friction is included, Eqs. (80) and (85) are valid only for $0 \le \phi_0 \le \pi/2$. For $\phi_0 > \pi/2$, the radial component of the magnetic force $\mathbf{F}_{12} \cdot \hat{\mathbf{r}} = -\cos\phi$

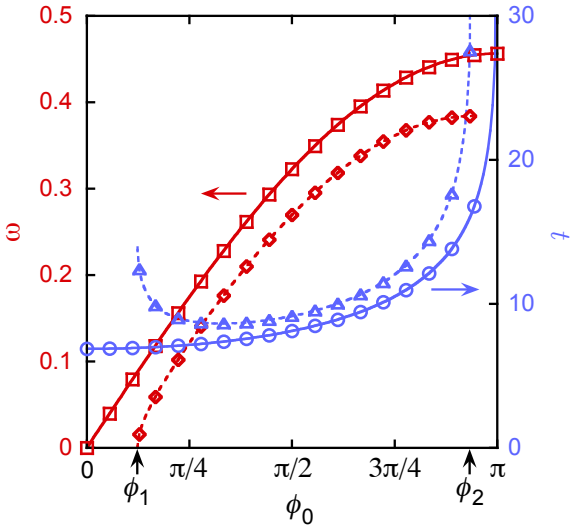

FIG. 7. Dimensionless angular speed ω and elapsed time t vs. initial angle ϕ_0 for a uniformly magnetized sphere that is allowed to spin at a fixed location $x = 4$ and $y = 0$ in response to the magnetic torque and the table friction torque. For ω, the solid trace and the squares are given respectively by Eq. (85) and *MagPhyx* software for $\gamma^* = 0$, and the dashed trace and the diamonds are given by Eq. (85) and *MagPhyx* software for $\gamma^* = 0.001$. For t, the solid trace and the circles are given by Eq. (84) and *MagPhyx* for $\gamma^* = 0$, and the dashed trace and the triangles are given by Eq. (84) and *MagPhyx* for $\gamma^* = 0.001$. Also shown are the limiting angles ϕ_1 and ϕ_2 given by Eqs. (91) and (92).

that provides the normal force for magnet-magnet kinetic friction [Eqs. (46) and (59)] is repulsive, hence there is no magnet-magnet friction force or torque at these angles.

Considering just magnet-magnet friction by setting $\gamma^* = \eta^* = 0$ in Eq. (80) reveals that the magnitude of the magnet-magnet friction torque exceeds the magnitude of the magnetic torque for small angles $\phi < \tan^{-1}(3\mu_m/2) = 0.214\pi$. For these angles, magnet-magnet friction can stop the rotation, after which static friction takes over and exactly balances the magnet torque. Figure 6 shows values of ω and t for $\mu_m = 0.53$ and $\phi_L < \phi_0 < \pi/2$. The lower limit ϕ_L can be obtained by setting $\omega = 0$ and $\phi_0 = \phi_L$ in Eq. (85), giving

$$1 - \cos\phi_L = \frac{3\mu_m}{2}\sin\phi_L. \tag{90}$$

Inserting $\mu_m = 0.53$ and solving numerically gives $\phi_L = 0.428\pi$, where $\omega = 0$ and t has a large negative slope in Fig. 6. For ϕ_0 satisfying $\phi_L < \phi_0 < \pi/2$, the sphere has sufficient angular momentum to overcome small-angle friction and reach the zero crossing at $\phi = 0$. For $\phi_0 < \phi_L$, magnet-magnet friction stops the sphere before it reaches $\phi = 0$.

We now investigate the role of friction at the larger separation $x = 4$, where the magnetic torque is much smaller and magnet-magnet friction is irrelevant because the spheres are not in contact. At this separation, Eqs. (86)

and (80) imply that the table friction torque is of order 20% of the magnetic torque magnitude, while the eddy torque is of relative order 7×10^{-6}.

Figure 7 shows the results for ω and t with and without table friction, for $\mu_m = \eta^* = 0$ and $x = 4$. Without table friction ($\gamma^* = 0$), the results look similar to Fig. 5, except that ω is smaller and t larger in Fig. 7 because the magnetic torque is weaker.

With table friction ($\gamma^* = 0.001$), ϕ_0 is restricted to the range $\phi_1 < \phi_0 < \phi_2$. The lower limit ϕ_1 given by setting $\phi_0 = \phi_1$ and $\omega = 0$ in Eq. (85), giving

$$1 - \cos\phi_1 - 3x^3\gamma^*\phi_1 = 0. \tag{91}$$

Solving this equation numerically for $x = 4$ and $\gamma^* = 0.001$ gives $\phi_1 = 0.124\pi$, where ω vanishes and t has a large negative slope. For $\phi_0 < \phi_1$, table friction stops the rotation before the zero crossing can be achieved.

The upper limit ϕ_2 is given by setting $\phi = \phi_2$ and $d\omega_z/dt = 0$ in Eq. (80), giving

$$-\sin\phi_2 + 3x^3\gamma^* = 0. \tag{92}$$

Solving this equation numerically for $x = 4$ and $\gamma^* = 0.001$ gives $\phi_2' = 0.061\pi$ and $\phi_2 = 0.939\pi$, supplementary angles at which the net torque is zero. Outside the range $\phi_2' < \phi < \phi_2$, the kinetic friction torque exceeds the opposing magnetic torque on sphere 2, and static friction succeeds in preventing any rotation of a sphere released from rest. Here, we assume for simplicity that the coefficient of static friction equals the coefficient of kinetic friction. The upper value ϕ_2 sets the upper limit on ϕ_0 because sphere 2, released from rest at $\phi_0 > \phi_2$, is unable to overcome static friction and begin rotating. The lower value ϕ_2' does not serve as the lower limit on ϕ_0 because it is smaller and less restrictive than the actual lower limit, ϕ_1. Released at an angle ϕ_0 satisfying $\phi_1 < \phi_0 < \phi_2$, sphere 2 has sufficient angular momentum to carry it through the zero crossing, including through the range $0 < \phi < \phi_2'$ where the kinetic friction torque exceeds the magnetic torque.

In summary, magnet-magnet friction plays a role when the spheres are in contact, table friction plays a role at large sphere separations, and eddy currents are always negligible.

VII. *MAGPHYX* SOFTWARE

We have built magnet simulation and visualization software for education, exploration, and discovery that integrates Eqs. (63)-(68) using fourth-order Runge-Kutta with fixed step size, for a free sphere (sphere 2) moving in two dimensions in response to the fields of a fixed sphere (sphere 1). Visualization of force, velocity, torque, angular velocity, magnetic moments, and magnetic fields aid in the understanding of magnet interactions. We make the software freely available as an interactive, animated web page called *MagPhyx*, and invite students and educators to take advantage of this learning and exploration tool [6]. *MagPhyx* is written in WebGL and is fully validated; its results appear as data points in Figs. 4-7, which agree with our independent calculations to within 0.1%.

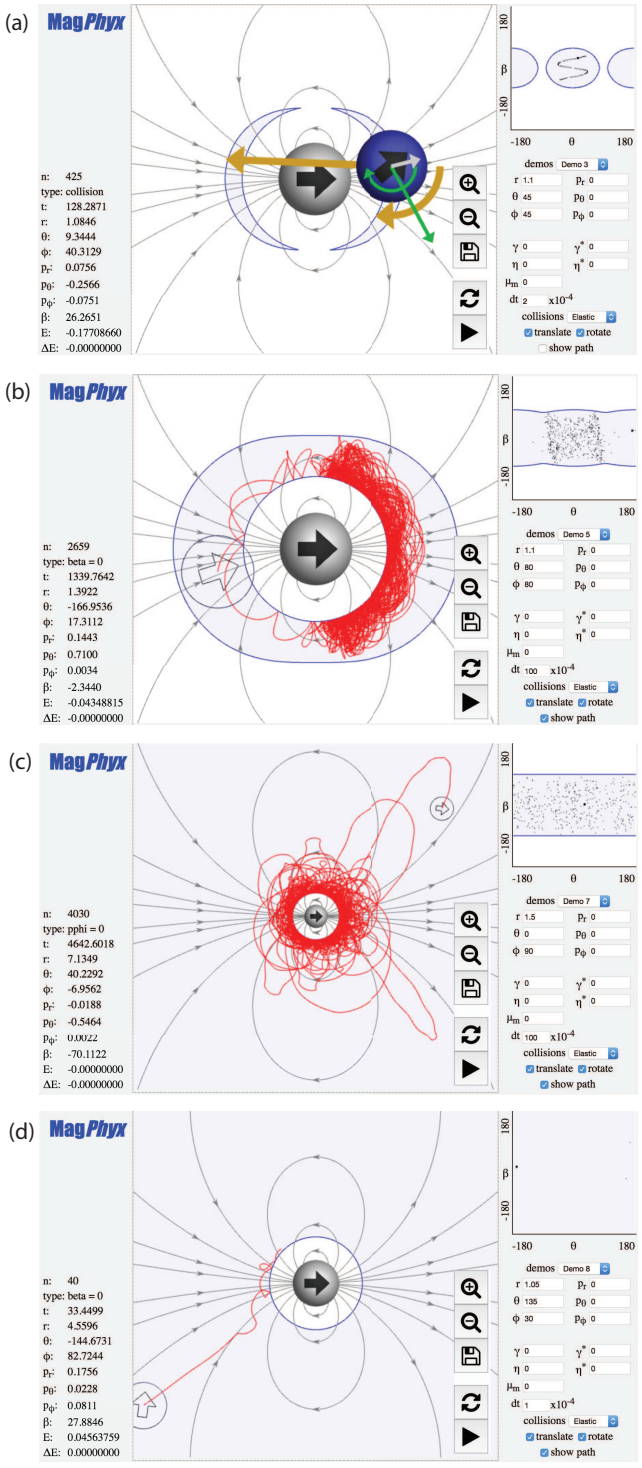

FIG. 8. *MagPhyx* screenshots from demos 3, 5, 7, and 8 (Sec. VII D).

A. Visualization and Controls

Figure 8 shows four *MagPhyx* screenshots that illustrate its capabilities and its predictions. The fixed sphere is shown as a shaded grey disk at the center of the main window, with the direction of its magnetic moment denoted by a black arrow at the center of the disk, and its magnetic fields denoted by directed grey traces emanating from and entering the disk.

If "show path" (lower right corner of screen) is not checked, the free sphere is shown as a disk whose color is determined by the dimensionless potential energy $U(r, \theta, \phi)$ of Eq. (38). Negative potential energies are denoted by a blue disk, with lower values denoted by deeper blue colors [Fig. 8(a)]. Positive potential energies are denoted by a red disk, with higher values denoted by deeper red colors. The direction of the magnetic moment of the free sphere is denoted by a black arrow atop the disk. Also atop the disk are shown a light grey arrow indicating the direction of the magnetic field at the center of the sphere, a green arrow representing velocity, and a green arc representing angular velocity. Shown just outside of the disk are a gold arrow representing force and a gold arc representing torque. To enable visualization over a wide range of these physical quantities, we take the length of the force vector to be proportional to the fourth root of the force magnitude, the length of the torque arc to be proportional to the cubed root of the torque magnitude, and the lengths of the velocity arrow and the angular velocity arc to be proportional to the square roots of the magnitudes of these quantities.

If "show path" is checked, the path of the center of the free sphere is shown as a red trace, and only outlines of the sphere and its magnetic moment vector are shown [Fig. 8(b-d)]. The other arrows and arcs are not shown in order to better see this path. The "show path" checkbox may be checked and unchecked during a simulation. Paths are saved whether or not the box is checked, so that when it is checked, all of the previous history of the simulation is shown.

The five control buttons on the main window are used to zoom in, zoom out, save, reset, and play/pause the simulation. The "save" button saves a log file with information about events (see below).

B. Input

Input parameters are shown at the lower right corner of the screen:

The "demo" menu gives sets of input parameters to demonstrate various physical principles discussed in this paper, and may be used to begin exploring the physics of magnet-magnet interactions. Selecting one of these demonstrations sets all of the input parameters for that demonstration. To run a demonstration, select it from the demo menu and press the "play" button.

Three dimensionless coordinates and three dimensionless momenta of the free sphere constitute the dynamical variables of the problem. They are: its radial coordinate $r \geq 1$ measured in units of the sphere diameter, its azimuthal position θ measured in degrees counterclockwise from the $+x$ axis, the orientation ϕ of its magnetic moment measured in degrees counterclockwise from the $+x$ axis (Fig. 2), its radial momentum $p_r = \dot{r}$, its orbital angular momentum $p_\theta = r^2\dot{\theta}$, and its spin angular momentum $p_\phi = \dot{\phi}/10$ [Eqs. (40)-(42)]. Values for the initial coordinates and momenta may be entered in the boxes on the lower right corner of the screen.

Alternatively, the initial position may be specified by clicking the mouse at the desired location of the free sphere, or by clicking and dragging the image of the sphere to the desired location. The initial magnetic orientation of this sphere may be specified by holding down the shift key and dragging the mouse in a circular arc until the desired orientation is achieved.

The dimensionless friction coefficients, together with estimates of these coefficients for Zen Magnets, are: the table friction coefficients $\gamma = 0.001$ and $\gamma^* = 0.001$ given by Eqs. (53) and (61), the eddy friction coefficients $\eta = 0.02$ and $\eta^* = 0.005$ given by Eqs. (54) and (62), and the magnet-magnet friction coefficient $\mu_m = 0.53$ given by Eq. (55). These estimates await experimental verification.

Governing the speed and accuracy of the simulations is the dimensionless Runge-Kutta time-step dt. For simulations used to validate the code in simple cases (Figs. 4-7), we used $dt = 1 \times 10^{-4}$, which gives results that are accurate to 0.1%. Smaller values of dt give more accurate results, while larger values give faster simulations.

The "collisions" menu refers to collisions of the free sphere with the fixed sphere, and enables either elastic or inelastic collisions. The "elastic" option gives perfectly elastic hard-sphere collisions for which the free sphere bounces off of the fixed sphere with T, p_θ, and p_ϕ unchanged, and with $p_r \to -p_r$, that is, with the angle of incidence equaling the angle of reflection. The inelastic option gives perfectly inelastic collisions for which the free sphere loses all of its radial momentum ($p_r = 0$) and some of its energy after the collision, with p_θ and p_ϕ unchanged. *MagPhyx* uses a binary search procedure, and time steps that are smaller than dt, to locate collisions precisely: if a time step causes the free sphere to overlap with the fixed sphere, shorter and shorter time steps are used to zoom in on the collision until a specified accuracy is reached.

The "translate" checkbox determines whether the free sphere is permitted to translate in response to forces. If unchecked, the sphere will remain in place. The "rotate" checkbox determines whether the free sphere is permitted to rotate in response to torques. If unchecked, the sphere will not rotate. Normal operation is with "translate" and "rotate" both checked. These checkboxes were used to validate the code (Sec. VI).

C. Output

To investigate nonlinear dynamical behavior and to enable convenient replication of behaviors discovered in the middle of long simulations, *MagPhyx* logs the values of dynamical variables at seven different event types, including collisions (when r reaches the value $r = 1$ from above), $\theta = 0$ events, $\phi = 0$ events, $p_r = 0$ events (excluding collisions), $p_\theta = 0$ events, $p_\phi = 0$ events, and $\beta = 0$ events. Here, $\beta = \phi - \phi_m$ is the angle between the magnetic moment of the free sphere and the local magnetic field given by Eq. (36).

This log file has 12 columns: the event number n, the event type, the time t of the event, and the corresponding values of the dimensionless variables r, θ, ϕ, p_r, p_θ, p_ϕ, β, E, and ΔE, where $E = T + U$ is the total dimensionless energy given by Eq. (37) and, and $\Delta E = E - E_0$ is the difference between the current energy and its initial value E_0. For long simulations without friction, small ΔE is an indicator of numerical accuracy. For simulations with friction, ΔE measures the extent of dissipation. Values of these 12 quantities are also displayed in the lower left corner of the screen.

Also shown on the upper right corner of the screen is an event map of values of β vs. θ at collision events, with each event represented by a small black dot on the screen. Shown as light blue shaded regions in this event map, and in the main window, are domain boundaries on β and r [31].

D. Demonstrations

A sampling of dynamical behaviors and program features may be selected from a pull-down menu in *MagPhyx*. For each demo, the free sphere is released from rest at a particular initial position and orientation, and is allowed to move in response to the magnetic force and torque of the fixed sphere. Hard-sphere elastic collisions are used and friction is ignored except for Demo 6, which includes perfectly inelastic collisions, table friction, and magnet-magnet friction. The descriptions below are labeled (in italics) by the characteristics of the initial force on the free sphere, according to the five force categories discussed in Sec. III.

Demo 1: *Attractive, central force with parallel collinear moments.* This initial condition gives a bound periodic orbit with the free sphere oscillating along the x axis and colliding elastically once per period with the fixed sphere, with the south pole of the free sphere contacting the north pole of the fixed sphere during each collision [Fig. 3(a) A].

Demo 2: *Attractive, central force with antiparallel noncollinear moments.* This initial condition gives a bound periodic orbit with the free sphere oscillating along the y axis and colliding elastically once per period with the fixed sphere. The spheres collide at points on their magnetic equators, with the north pole of the fixed sphere attracting the south pole of the free sphere, and the south pole of the fixed sphere attracting the north pole of the free sphere. [Fig. 3(e) C].

Demo 3: *Attractive, oblique force with a discontiguous domain: "S" pattern.* This initial condition gives a bound, apparently nonperiodic orbit with the free sphere confined to the right half plane. Although the orbit does not appear to repeat itself over many hundreds of collisions, the β vs. θ map shows intriguing "S"-shaped structure [Fig. 3(b) B].

Demo 4: *Attractive, oblique force with a discontiguous domain: zig-zag pattern.* This high-speed simulation shows the path of a bound, apparently nonperiodic orbit with the free sphere confined to the right half plane. This orbit shows an intricate zig-zag pattern in the β vs. θ map.

Demo 5: *Attractive, oblique force with a contiguous domain.* This high-speed simulation shows the path of a bound, apparently nonperiodic orbit with the free sphere confined to the right half plane for hundreds of events, then moving to the left half plane. This orbit fills in much of the domain in the β vs. θ map.

Demo 6: *Attractive, oblique force with friction and inelastic collisions.* This simulation has a domain that is contiguous initially and shrinks slowly as energy dissipates through table friction. When the free sphere collides inelastically with the fixed sphere, the energy drops abruptly to a lower value and the domain becomes discontiguous. Thereafter, the domain shrinks slowly as energy dissipates through magnet-magnet friction and table friction until the free sphere settles near the minimum-energy state, with the south pole of the free sphere near the north pole of the fixed sphere. Magnet-magnet friction prevents the free sphere from actually reaching this state [Sec. VI B, Fig. 3(a) B].

Demo 7: *Perpendicular force at the infinite domain threshold.* This high-speed simulation shows the path of a chaotic orbit with energy $E = 0$, the threshold between bound and unbound orbits. The free sphere takes long excursions from the fixed sphere, but always returns because it lacks the energy to escape fully from the fixed sphere. To enable viewing of the free sphere during its long excursions, the simulation is shown zoomed out [Fig. 3(c) A].

Demo 8: *Repulsive, oblique force.* This initial condition gives an unbounded orbit in which the free sphere makes three collisions with the fixed sphere and

then embarks on a long, linear journey to infinity, never to return.

Demo 9: *Repulsive, central force with antiparallel collinear moments.* In this simulation, the north pole of the free sphere makes initial contact with the north pole of the fixed sphere, which repels the free sphere to infinity along the $+x$ axis [Fig. 3(e) A].

Demo 10: *Repulsive, central force with parallel non-collinear moments.* In this simulation, a point on the equator of the free sphere makes initial contact with a point on the magnetic equator of the fixed sphere. The north pole of the fixed sphere repels the north pole of the free sphere, the south pole of the fixed sphere repels the south pole of the free sphere, and the free sphere travels to infinity along the $+y$ axis [Fig. 3(a) C].

E. Results

With its force, torque, velocity, and angular velocity visualizations, *MagPhyx* is particularly well suited to illustrate basic principles of inertia. A force in a particular direction does not mean that the free sphere moves in that direction; it means that the change in its linear momentum is in that direction [Fig. 8(a)]. Similarly, a torque in a particular direction does not mean that the sphere turns in that direction; it means that the change in its angular momentum is in that direction. A torque that acts to align $\mathbf{m}_2$ with $\mathbf{B}_1$ can eventually lead to angular momentum that acts to align these vectors. But the very angular momentum that carries $\mathbf{m}_2$ into alignment with $\mathbf{B}_1$ continues to rotate the sphere in the same direction until $\mathbf{m}_2$ is out of alignment with $\mathbf{B}_1$ again, when a torque in the opposite direction begins to slow the rotation in an attempt to bring the sphere back into alignment. In the absence of dissipation, such oscillations can continue indefinitely. These oscillations are an integral part of demonstrations 4, 5, 7, and 8. (Selecting a value of dt of about $dt = 1 \times 10^{-4}$ is needed to observe these oscillations in demonstrations 4, 5, and 7.) In a similar way, forces that strive to bring the sphere into regions where $\mathbf{m}_2$ is better aligned with $\mathbf{B}_1$ give it linear momentum that can carry the sphere beyond these regions.

VIII. CONCLUSIONS

We exploit the equivalence of the force between point dipoles to the force between spheres to investigate the time-dependent interactions between two magnet spheres, with one held fixed. We find both bound and unbound states, with the free sphere confined to one of two discontiguous domains for bound states at low energies, and with these domains merging for high-energy bound states. We investigate three different mechanisms of energy dissipation through non-conservative forces, and determine when they are relevant. We offer a magnet interaction software tool called *MagPhyx* to the community for use in teaching and exploration.

The 2D conservative problem has three coordinates and three momenta: radial momentum, orbital angular momentum, and spin angular momentum. Because none these momenta is conserved, energy may be exchanged between magnetic potential energy, translational kinetic energy, and rotational kinetic energy. This exchange leads to rich nonlinear behavior, including both periodic and non-periodic orbits shown in the demonstrations above. We intend to investigate this behavior further, by exploring the stability of fixed points and periodic orbits, searching for non-trivial periodic orbits, and characterizing bound chaotic orbits [31].

The tools presented in this paper may be used to investigate the stability of magnet configurations used in building shapes using magnet spheres. These tools may also be used in the classroom and teaching laboratory to investigate the magnetic fields produced by chains of magnets of different lengths, and the energies of symmetric rings of magnets of different lengths. The point-sphere equivalence may assist in research on arrays of nanoparticles and permanent magnets, in dynamic simulations of magnet sphere interactions, and in applications in science education.

Experiments with real magnets could be used to refine our friction-coefficient estimates and to test our predictions of dynamical behavior. One approach is to take high-speed videography of a magnet released from various positions on a horizontal surface, with its poles labeled, in the presence of a second magnet that is held fixed on the surface. Using magnets larger than 5 mm in diameter might help to facilitate such measurements.

IX. ACKNOWLEDGMENTS

We gratefully acknowledge support from NSF Grant No. 1332265.

[1] David A. Richter, Expert Report, "Teaching Geometry with Magnet Sphere Kits," in the matter of Zen Magnets, LLC, CPSC Docket No. 12-2, Item 124, Exhibit

3, 10/20/2014, http://www.cpsc.gov/en/Recalls/Recall-Lawsuits/Adjudicative-Proceedings/ (accessed Feb. 9, 2016).

[2] Boyd F. Edwards, "Expert Report: Educational Value of Neodymium Magnet Spheres in the matter of Zen Magnets, LLC, CPSC Docket No. 12-2," Item 124, Exhibit 4, 10/20/2014, http://www.cpsc.gov/en/Recalls/Recall-Lawsuits/Adjudicative-Proceedings/ (accessed Feb. 9, 2016). Redacted, high-resolution, color version available at https://drive.google.com/file/d/0Bw7DdocNZGQgWThTb3VvUHYza2s/view (accessed May 10, 2016).

[3] The Zen Gallery, curated by Shihan Qu, http://zenmagnets.com/gallery/ (accessed Feb. 9, 2016).

[4] Typing "Zen Magnets" into the YouTube search field at https://www.youtube.com identifies over 90,000 videos describing various (accessed Mar. 23, 2016). As of August 22, 2014, the most popular of these had a total view count exceeding 145 million (Ref. [2], Appendix D).

[5] Boyd F. Edwards, D. Mark Riffe, Jeong-Young Ji, and William A. Booth, "Interactions between uniformly magnetized spheres," to be published.

[6] John M. Edwards, *MagPhyx* Software, http://www2.cose.isu.edu/∼edwajohn/MagPhyx (accessed Mar. 11, 2016).

[7] Beginners Simulation Tool Needed, ENGTIPS.COM Engineering Forums, http://www.engtips.com/viewthread.cfm?qid=261809 (accessed Mar. 22, 2016).

[8] "Simulating toy magnet balls? (eg: Zen Magnets)," http://www.physicsforums.com/showthread.php?t=596513 (accessed Feb. 9, 2016).

[9] Wikipedia, *Force between magnets*, https://en.wikipedia.org/wiki/Force_between_magnets (accessed Feb. 10, 2016).

[10] Commercial magnetic-field mapping software can be found at phttp://www.gmw.com/magnetic_measurements/magmap.html?gclid=CLuJiK_NvssCFUKUfgodK9AAJg, https://www.integratedsoft.com, http://www.infolytica.com (accessed Feb. 16, 2016).

[11] PhET interactive simulations, University of Colorado at Boulder, https://phet.colorado.edu/en/simulations /category/physics (accessed Mar. 15, 2016).

[12] Several countries, including the United States, have banned the sale of 5-mm diameter nickel-coated neodymium magnets marketed as a desk toys under the trade names BuckyBalls, Zen Magnets, Neoballs, etc. following reports of intestinal injuries from ingestion of these magnets. But 2.5-mm magnets may be still be purchased at http://micromagnets.com (accessed Feb. 16, 2016), and magnet spheres of various sizes, including 5-mm spheres, may still be purchased from industrial suppliers (http://www.kjmagnetics.com/, http://www.alibaba.com, http://www.magnet4less.com, accessed Feb. 16, 2016).

[13] YouTube channel, Boyd Edwards, https://www.youtube.com/channel/UCEe7mMyWdy1GuX6fQUHUUQw/videos (accessed Mar. 22, 2016).

[14] Roald K. Wangsness, *Electromagnetic Fields*, 2nd edition (Wiley, New York, NY, 1986), p. 326.

[15] J. D. Jackson, *Classical Electrodynamics*, 2nd edition (Wiley, New York, NY, 1975), p. 195.

[16] David Griffiths, *Introduction to Electrodynamics*, 3rd edition (Pearson Education, Delhi, India, 1999), p. 246.

[17] David J. Griffiths, "Dipoles at rest," Am. J. Phys. **60**, 979-987 (1992).

[18] Neodymium magnets have thin metallic coatings, and therefore depart from uniform spheres. Taking these coatings into account in calculating the moment of inertia leads to corrections that are less than 1%. We therefore treat the spheres as solid, uniform spheres for convenience. For reference, the densities of Nd alloy, Cu, and Ni are 7.3 g/cm^3, 9.0 g/cm^3, and 8.9 g/cm^3, respectively, and the Ni-Cu-Ni coatings on 5.00-mm diameter spheres have thicknesses 0.015 mm, 0.025 mm, and 0.010 mm, respectively (Sec. IV).

[19] The vector magnetic fields shown in Fig. 3 are courtesy Wikipedia and Wikimedia Commons, https://en.wikipedia.org/wiki/File:VFPt_dipole_point.svg (accessed Feb. 16, 2016).

[20] Roald K. Wangsness, *Electromagnetic Fields*, 2nd edition (Wiley, New York, NY, 1986), p. 494.

[21] Horace Lamb, *Hydrodynamics* 16th edition (Dover, New York, 1993) Sec. 337, pp. 597-599.

[22] Magnetic Properties, Integrated Magnetics, http://www.intemag.com/magnetic_properties.html (accessed Feb. 27, 2016).

[23] Neodymium Magnet Physical Properties, K&J Magnetics, Inc., https://www.kjmagnetics.com/specs.asp (accessed Feb. 27, 2016).

[24] Wikipedia, *Electrical resistivity and conductivity*, https://en.wikipedia.org/wiki/Electrical_resistivity_and_conductivity (accessed March 7, 2016).

[25] Shihan Qu, Zen Magnets, private communication, Mar. 2, 2016.

[26] G. Aubert, J.-F. Jacquinot, and D. Sakellariou, "Eddy current effects in plain and hollow cylinders spinning inside homogeneous magnetic fields: Application to magnetic resonance," J. Chem. Phys. **137**, 154201 (2012).

[27] A. Jassal, H. Polinder, J. A. Ferreira, "Literature survey of eddy-current loss analysis in rotating electrical machines," IET Electr. Power Appl., 2012 **6** (9), 743-752 (2012).

[28] Min-Gyu Park, Jang-Young Choi, Hyeon-Jae Shin, and Seok-Myeong Jang, "Torque analysis and measurements of a permanent magnet type Eddy current brake with a Halbach magnet array based on analytical magnetic field calculations," J. Appl. Phys. **115**, 17E707 (2014).

[29] L. Landau, E. Lifchitz, and L. P. Pitaevskii, *Electrodynamics of Continuous Media* (Pergamon, Oxford, 1960), Sections 63 and 64, pp. 217-223.

[30] Coefficients of Friction, Applied Industrial Technologies, http://www.applied.com/site.cfm/CoefficientsofFriction.cfm, (accessed Mar. 15, 2016).

[31] Boyd F. Edwards and John M. Edwards, to be published.